THE JOURNAL OF PHYSICAL CHEMISTRY C

Article

pubs.acs.org/JPCC

Long-Range Periodicity of S/Au(111) Structures at Low and Intermediate Coverages

P. N. Abufager,*[,†,‡] G. Zampieri,[‡,§,∥] K. Reuter,[⊥] M. L. Martiarena,[‡,§] and H. F. Busnengo[†,‡]

[†]Instituto de Física de Rosario and Universidad Nacional de Rosario, Av. Pellegrini 250 (2000) Rosario, Argentina

[‡]Consejo Nacional de Investigaciones Científicas y Técnicas (CONICET) , Sarmiento 440, Buenos Aires, Argentina

[§]Centro Atómico Bariloche, Av. Bustillos 9500, 8400 San Carlos de Bariloche, Argentina

[∥]Instituto Balseiro, Universidad Nacional de Cuyo, Bariloche, Río Negro, Argentina

[⊥]Department Chemie, Technische Universität München, Lichtenbergstraße 4, D-85747 Garching, Germany

Supporting Information

ABSTRACT: Through a systematic analysis based on DFT calculations, we have studied the adsorption of S atoms on Au(111) at low and intermediate coverages ($\theta \leq 1/3$). Our calculations predict ground state structures characterized by two periodicities: (5×5) and $(\sqrt{3} \times \sqrt{3})R30°$. In line with experiments, the (5×5) periodicity seems to dominate in a much larger coverage range than the $(\sqrt{3} \times \sqrt{3})R30°$ one, which should be only observable in a narrow coverage window close to 1/3. In addition, our results unambiguously reveal the crucial role of S-induced substrate relaxation. Using a first-principles parametrized lattice-gas Hamiltonian approach, we determine lateral interactions between S atoms which allow us to provide a sound explanation for the relative stability of ground state structures.

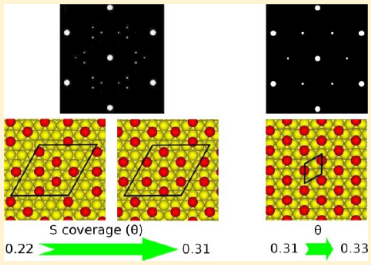

INTRODUCTION

The interaction of sulfur atoms with metal surfaces has attracted a great deal of attention during the last years. Sulfur adsorbates provoke a fast deactivation of metal-based catalysts[1] and affect the composition and structure of self-assembled monolayers of S-containing organic molecules such as thiols.[2,3] On Au(111), a S adlayer can be formed by immersion in sulfide-containing solutions (S_2^-, SH^-,[4] H_2S[5]) or by sample exposure to gaseous S_2[1,6] or SO_2.[7,8] Irrespective of the exposure method, S atoms covalently chemisorb on Au(111), and form various structures depending on the coverage, θ (defined as the ratio of the number of S adsorbates and the number of topmost-layer Au atoms). For $\theta \gtrsim 0.4$, the S−Au(111) system exhibits complex phases[1,6,9−13] whose structures had been a matter of debate, in particular about their nature as either S-adlayers[9,11,13] or gold sulfide films[10,12] which in turn, depend on the temperature conditions of the experiments.[12] In contrast, for $\theta = 1/3$ S atoms form a *simple* well-ordered $(\sqrt{3} \times \sqrt{3})R30°$ adlayer with all the S atoms adsorbed on equivalent three-fold hollow sites.[1,4,6,14,15] However, whereas this phase has been observed in electrochemical environments at room temperature (RT),[4] in ultra-high vacuum (UHV) conditions its stability seems to be restricted to lower temperatures.[6,10] For lower coverages, the typical observed low-energy electron diffraction (LEED) pattern corresponds to a S adlayer characterized by a (5×5) periodicity with three spots symmetrically positioned around the location expected for the 1/3 order beams of a $(\sqrt{3} \times \sqrt{3})R30°$ ordering.[6,14,15] Such a quite peculiar LEED pattern (hereafter referred to as split-$(\sqrt{3})$ has been associated to a 7-S atoms *rosette*-motif with (5×5) periodicity.[6] This structure is characterized by groups of 7 S atoms at distances $d_{S-S} = \sqrt{3}\Delta$ (Δ being the nearest neighbor surface Au−Au distance). Interestingly, in contrast with the marginal stability of the $(\sqrt{3} \times \sqrt{3})R30°$ structure in UHV, the split-$\sqrt{3}$ LEED pattern has been observed for many surface preparations (giving rise to somewhat different S coverages) and in a wide range of temperatures (up to ∼670 K).[6]

Even though extracting conclusions about the lateral interactions from LEED experiments is (if possible) extremely complex, the marginal stability of the $(\sqrt{3} \times \sqrt{3})R30°$ structure might be thought of as an indication of a slightly repulsive interaction between second nearest neighbor (2NN) S atoms. Unfortunately, the available theoretical results do not further clarify this issue. Density Functional Theory (DFT) calculations for S/Au(111) at low S coverages have been mainly focused on the electronic structure of the system for a few structures, none of them capable of accounting for the split-$\sqrt{3}$ LEED pattern observed in experiments.

In this work we perform a systematic analysis based on DFT calculations for the S/Au(111) interface at low and intermediate coverages ($\theta \leq 1/3$). We have explored many possible S/Au(111) structures, characterized by $(n \times n)$ periodicities with $1 \leq n \leq 6$. In line with LEED experimental data,[6] our results predict a ground state curve of the system characterized by a (5×5) periodicity in a much larger coverage range than by the $(\sqrt{3} \times \sqrt{3})R30°$ one, which is expected to

Received: August 20, 2013
Revised: December 8, 2013
Published: December 10, 2013

prevail only in a 0.02 width θ-window close to 0.33. In addition, from the comparison of binding energies computed with and without surface relaxation upon adsorption, and the development of a lattice gas Hamiltonian model[16−22] for S/Au(111), we have found that the lateral interactions between S atoms present the following main properties: (i) weak attraction for $d_{S-S} \approx 15$ Å which contributes to the stability of structures with (5×5) periodicity, (ii) shorter but still long-ranged S−S repulsion due to the elastic response of the Au(111) surface, which is maximum for $d_{S-S} \approx 9$ Å, and being the major source of instability of the $(\sqrt{3} \times \sqrt{3})$ structure, (iii) very small repulsion (if any) between 2NN S adsorbates (i.e., $d_{S-S} \approx 5$ Å) which helps to understand the high stability of the *rosette-like* motif, and (iv) large short-range (presumably electrostatic) repulsion (i.e., $d_{S-S} \approx 3$ Å) which prevents structures with first nearest neighbor (1NN) S atoms.

THEORY

Determination of Ground State Structures. Let us consider a set of N sulfur atoms adsorbed on an ideal Au(111) surface of area A, with N_m metal atoms in the topmost layer. Thus, $\theta = N/N_m$ and the total adsorption energy is N times the average adsorption energy per adsorbate, ε, which depends on the positions of the adsorbates.

Though the ground state (GS) of the system does not depend on how the adsorbates have been deposited, if the S adsorbates are produced through dissociative adsorption of S_2 molecules, it is reasonable to define and compute ε as follows:

$$\varepsilon = \frac{1}{N}\left[E_{NS@Au(111)} - E_{Au(111)} - \frac{1}{2}NE_{S_2}\right] \quad (1)$$

In eq 1, $E_{NS@Au(111)}$, $E_{Au(111)}$, and E_{S_2} are the total energies of the NS/Au(111) system, the clean Au(111) surface, and S_2 in vacuum, respectively. A negative ε indicates that the adsorption is exothermic with respect to the clean surface and S_2 molecule. For a given coverage θ, among all the possible configurations that the N adsorbates can form on the surface, the GS of the system is the one with the lowest ε value. The GS can be a single domain covering the whole surface or a set of domains characterized by different *local* coverages (lower and greater than θ) which all together give rise to a *total* coverage θ.

Let us consider a structure with a total coverage θ composed by only two domains i and j, locally characterized by coverages θ_i and θ_j $(0 \le \theta_i \le \theta \le \theta_j)$ and average adsorption energies per adsorbate ε_i and ε_j, respectively. In this context, ε_i refers to the average binding energy per adsorbate for a single domain i that covers the whole surface.[23] Denoting with N_k $(k = i,j)$ the number of adsorbates in the domain k $(N_i + N_j = N)$, the average adsorption energy per adsorbate of such a two-domain structure is:

$$\varepsilon_{ij}(\theta) = \frac{N_i\varepsilon_i + N_j\varepsilon_j}{N} \quad (2)$$

By using eq 2 we neglect the effect of the interdomain boundaries which is valid for the large domains of interest for our purposes. Taking into account that the surface area covered by the domain k is

$$A_k = \frac{N_k/\theta_k}{N/\theta}A \quad (3)$$

$(A_i + A_j = A)$, it can be shown that:

$$\frac{A_i}{A} = \frac{\theta_j - \theta}{\theta_j - \theta_i}\frac{A_j}{A} = \frac{\theta - \theta_i}{\theta_j - \theta_i} \quad (4)$$

and

$$\varepsilon_{ij}(\theta) = \frac{\alpha_{ij}}{\theta} + \beta_{ij} \quad (5)$$

where

$$\alpha_{ij} = \frac{\theta_i\theta_j(\varepsilon_i - \varepsilon_j)}{\theta_j - \theta_i} \qquad \beta_{ij} = \frac{\theta_j\varepsilon_j - \theta_i\varepsilon_i}{\theta_j - \theta_i} \quad (6)$$

Interestingly, $\varepsilon_{ij}(\theta)$ is proportional to $1/\theta$, and if $\theta_i = 0$ (i.e., the domain i is a clean surface patch), $\alpha_{ij} = 0$; thus, $\varepsilon_{ij}(\theta) = \beta_{ij} = \varepsilon_j$, irrespective of the value of θ.

Let us consider now a single domain covering the whole surface characterized by a coverage, θ, and average adsorption energy per adsorbate, ε. For this monodomain structure to be the GS of the system, ε must not only be the smallest value among all the possible monodomains with the same coverage, θ, but must also hold $\varepsilon < \varepsilon_{ij}(\theta)$ for *any* pair of monodomains i,j with $\theta_i < \theta < \theta_j$. Otherwise, if there exist two monodomains i and j for which $\varepsilon_{ij}(\theta) < \varepsilon$, a two-domain structure ij (with fractional surface areas given by eq 4) is energetically more stable. In order to determine a *possible GS curve* connecting the lowest energy structures for various coverages, it is convenient to consider as many monodomains as possible, and then plot their ε values as a function of $1/\theta$ (see eq 5). An example of such a plot is shown in Figure 1 where the plus symbols

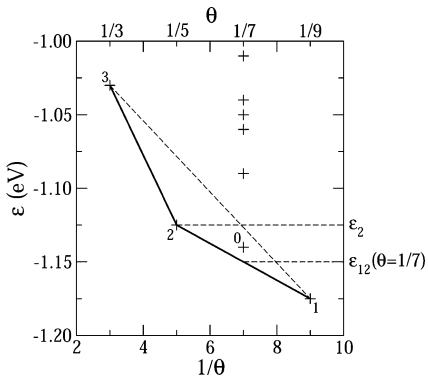

Figure 1. Schematic illustration of the idea behind the ground state line determined by adsorption energies as a function of $1/\theta$.

represent the ε values of several monodomains. In such a situation, though for $\theta = 1/7$ the monodomain **0** is the most stable one, it lies above the straight line connecting **1** and **2**. Therefore, there exists a two-domain structure with $\varepsilon_{12}(\theta = 1/7) < \varepsilon_0$, and then **0** is not the GS of the system for $\theta = 1/7$. In addition, Figure 1 also shows that for $\theta = 1/9$ the monodomain **1** is more stable than any configuration composed of islands of local structure **2** separated from each other by clean surface patches, because **1** lies below the horizontal dashed line $\varepsilon = \varepsilon_2$.

It is important to keep in mind that the previous analysis based on pure energetic arguments can only be used to predict structures in the limit of zero temperature. However, under realistic experimental conditions entropic effects can play a prominent role. In particular, configurational entropy favors the formation of relatively dense islands of adsorbates over homogeneous diluted (more extended) monodomains. This

dx.doi.org/10.1021/jp408340d | J. Phys. Chem. C 2014, 118, 290−297

is because, when a set of adsorbates is closer together, the others have more accessible sites over which to distribute. Thus, in contrast with the usual belief, configuration entropy can give rise to island formation even without attraction between adsorbates.[24] At a given temperature, the role of this configurational entropic effect increases when coverage decreases. Thus, at very low coverages and not too low temperatures they are expected to prevail over energetic factors. Unfortunately, a quantitative evaluation of Gibbs free energies of adsorption (including configurational entropy) is not a trivial task.[16−22] Still, even if the configurational entropic effect mentioned above prevails, the preferred islands are likely to be characterized by one of the local structures that define the GS curve. Therefore, the determination of the GS of an atom-surface system as a function of θ is very important as a complement of experiments intended to elucidate the structures formed by adsorbates well above 0 K.

Computational Details. Total energies of S interacting with Au(111) have been evaluated through DFT calculations within the generalized gradient approximation (GGA) proposed by Perdew and Wang (PW91),[25] using the Vienna Ab-initio Simulation Package (VASP).[26−31] The one-electron Kohn−Sham orbitals were expanded in a plane wave basis set with an energy cutoff of 350 eV and electron−ion interactions were described through ultrasoft pseudopotentials.[32] Core states were treated fully relativistically and, for the valence states, relativistic effects were included in a scalar relativistic treatment.[30,31]

The Au(111) surface was modeled by a five-layer slab and 15 Å of vacuum space to avoid the interaction with its periodic images. Sulfur atoms were adsorbed only on one side of the slab, and during full geometry optimizations we allowed relaxation of all the Au atoms in the three topmost layers and the S adsorbates until reaching forces smaller than 0.02 eV/Å. The first Brillouin Zone sampling was carried out according to the Monkhorst and Pack method[33] with meshes 13 × 13 × 1, and 9 × 9 × 1, for the unit cells (3 × 3), and (4 × 4) respectively, and 7 × 7 × 1 for the unit cells (5 × 5), $3\sqrt{3} \times 3\sqrt{3})R30°$, and (6 × 6). Electron smearing was introduced following the Methfessel−Paxton technique[34] with $N = 1$ and $\sigma = 0.2$ eV, and the energies were extrapolated to 0 K. We have carried out spin-restricted calculations, except for the S_2 molecule in vacuum. With the settings mentioned above, the calculated lattice constant for Au is $a_{calc} = 4.18$ Å which agrees well with the experimental value $a_{exp} = 4.08$ Å,[35] and the resulting binding energies per S adsorbate are converged within ∼0.01 eV (see the Supporting Information for details about the convergence tests).

RESULTS AND DISCUSSION

As a first step we have carried out full geometry optimizations for a single S atom initially located on the high symmetry sites of Au(111) (i.e., top, bridge, hollow-hcp, and hollow-fcc) within (2 × 2) and $(\sqrt{3} \times \sqrt{3})R30°$ unit cells (i.e., for $\theta = 1/4$ and $\theta = 1/3$, respectively). The most stable final configurations obtained correspond to the S atom adsorbed on hollow sites, with hollow-fcc more stable than hollow-hcp (in good agreement with previous DFT-GGA results[1,36]) by 0.18 and 0.17 eV for $\theta = 1/4$ and $\theta = 1/3$, respectively. We have also compared the total binding energy of structures with two S atoms per unit cell, either with the two S atoms on hollow-fcc sites (structures type-i shown in the upper panels of Figure 2), or with one S atom on a hollow-fcc site and the other on a hollow-hcp site (structures type-ii shown in the lower panels of Figure 2). These tests were carried out for the unit cells $(3 \times \sqrt{3})$ and (5 × 5) which correspond to S coverages $\theta = 1/3$ (left panels of Figure 2) and $\theta = 2/25$ (right panels of Figure 2), respectively. The total binding energy of the two type-i structures is smaller (adsorption is more stable) than for the corresponding type-ii one, by 0.12 eV for $\theta = 1/3$, and by 0.18 eV for $\theta = 2/25$. All these results indicate that for $\theta \leq 1/3$, adsorption on hollow-fcc sites is significantly more stable than on hollow-hcp. Then, our results predict that for $\theta \leq 1/3$, the GS of the S/Au(111) system involves adsorption on hollow-fcc sites only, in good agreement with Normal Incidence X-ray Standing Wavefield Absorption (NIXSW) results[6] and dynamical LEED analysis.[15] Accordingly, in what follows, the hollow-fcc site will be referred to as the *adsorption site*.

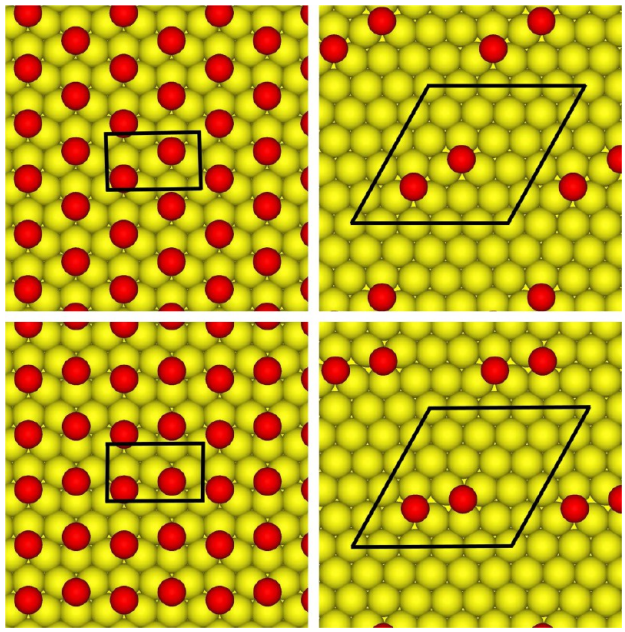

Figure 2. Schematic representation of S/Au(111) structures with two sulfur atoms per unit cells, corresponding to S-coverages $\theta = 1/3$ (left panels) and $\theta = 2/25$ (right panels). Upper (lower) panels illustrate type-i (type-ii) adsorption models (see text). The red and yellow balls are the S and Au atoms, respectively. The black lines represent the surface unit cells.

Concerning the S−S lateral interaction, we have found that adsorption of two S atoms on 1NN adsorption sites is largely unfavorable with respect to adsorption on 2NN sites. For instance, within a (5 × 5) unit cell, the total binding energy of two 1NN S atoms is larger (less stable) than for two 2NN S atoms by ∼0.4 eV. Such a large energy penalty clearly rules out the possibility of adsorption of S atoms on 1NN adsorption sites in the GS of S/Au(111) for the low coverages of interest in this work ($\theta \leq 1/3$). Thus, it is well justified to restrict the search of possible GS structures to those involving S atoms adsorbed only on hollow-fcc sites surrounded by six empty 1NN hollow-fcc sites (i.e., avoiding 1NN S atoms). This reduces significantly the number of *target structures*, and so we have been able to investigate *all* the possible structural models of S/Au(111) characterized by $\theta \leq 1/3$, in $(n \times n)$ unit cells with $n = 3$, 4, and 5 (47 structures). In addition, we have also carried out DFT calculations for 7 configurations in the unit cell $(3\sqrt{3} \times 3\sqrt{3})R30°$ for $5/27 \leq \theta \leq 1/3$, as well as a few extra calculations in bigger unit cells up to (6 × 6).

dx.doi.org/10.1021/jp408340d | J. Phys. Chem. C 2014, 118, 290−297

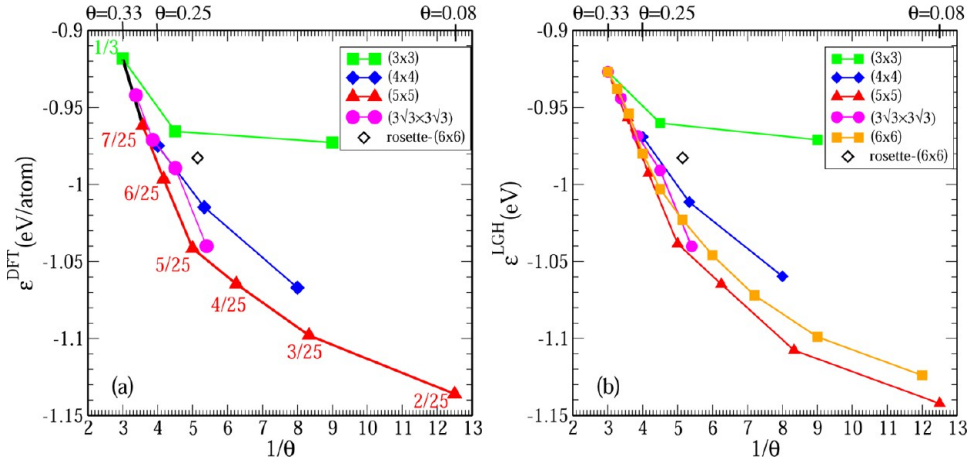

Figure 3. Adsorption energies for the most stable structures as a function of $1/\theta$. (a) DFT, (b) LGH (see text).

In Figure 3a we have represented the DFT average binding energy per S atom, ε^{DFT}, of the most stable structures found for each periodicity, as a function of θ^{-1} (the values for all the structures investigated are reported in the Supporting Information)[37] The straight lines connecting the lowest energy structures characterized by a given periodicity (e.g., (3×3), (4×4), etc.) have been drawn to facilitate the comparison of the stability of the various *families* of periodicities considered. It is important to mention that the structures $(\sqrt{3} \times \sqrt{3})R30°$ and (2×2) (with one S atom per unit cell) have also been considered as members of the (3×3) and (4×4) *families*, respectively.

Figure 3a shows that the (5×5) *family* is the most stable one in a wide range of coverages: $0.08 \leq \theta \leq 7/25 = 0.28$. The $(\sqrt{3} \times \sqrt{3})R30°$ periodicity begins to appear only above $\theta = 0.28$ coexisting with the configuration of 7 S atoms in a (5×5) unit cell. According to eq 4 the area covered with patches of $(\sqrt{3} \times \sqrt{3})R30°$ order increase linearly with θ and become the dominant phase for $\theta > (7/25 + 1/3)/2 = 0.31$. Thus, our calculations predict that this phase should be observable only in the narrow range of coverages $0.31 < \theta \leq 0.33$, in agreement with the experimental findings.[6,14,15]

The lowest energy (5×5) configurations found for $\theta = n/25$ with $n = 7$, 6, 5, 4, 3, and 2 are schematized in Figure 4.[38] These structures give rise to the GS curve of S/Au(111) for $2/25 \leq \theta \leq 7/25$. It is important to note that the lowest energy structure for $\theta = 7/25$ (the only one that avoids adsorption on 1NN sites in a (5×5) cell) is the 7 S atom *rosette* motif first proposed to explain the split-$\sqrt{3}$ LEED pattern.[6,14,15] Thus, the present results provide additional theoretical support to the structure determination of refs 6,15 based purely on LEED results.

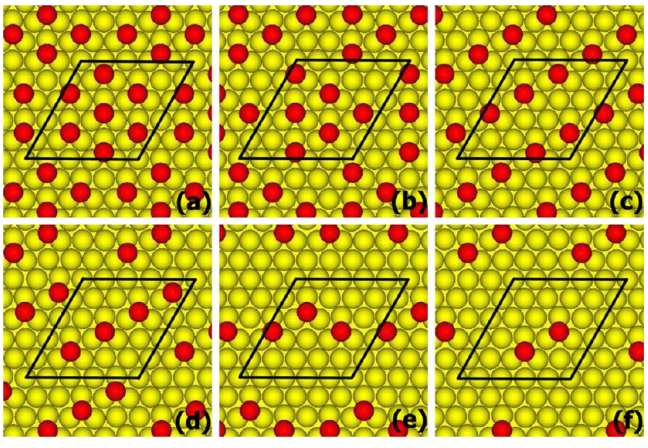

Figure 4. DFT lowest energy (5×5) configurations with n S atoms in a (5×5) unit cell ($\theta = n/25$) with $n = 7$ (a), 6 (b), 5 (c), 4 (d), 3 (e), and 2 (f).

Figure 4 shows that when the coverage increases, S atoms prefer to locate at a distance $d_{S-S} = \sqrt{3}\Delta$ from each other. In general, the lowest energy structure for each coverage is one of the configurations with higher number of 2NN S pairs. This suggests a relatively favorable S−S interaction for this particular distance which in principle, seems to be at odds with the relatively low stability of the $(\sqrt{3} \times \sqrt{3})R30°$ structure. We will come back to this issue below.

It might be argued that our DFT calculations have been mainly focused on periodicities shorter than or equal to (5×5), and that other unexplored structures characterized by larger cells might be even more stable. Though this suspicion is not supported by our DFT results for the $(3\sqrt{3} \times 3\sqrt{3})R30°$ unit cell (see Figure 3a), it would be desirable to extend our systematic study for even larger unit cells. Unfortunately, this entails a significant increase of the computational cost. For instance, in a (6×6) unit cell there are 44% more Au atoms than in the (5×5) one, and for the low coverages of interest here, the number of possible S/Au(111) structures becomes huge.

In order to investigate additional possible structures characterized by bigger unit cells we have parametrized a simple three-body lattice gas Hamiltonian (LGH) model (see e.g., refs 16−22). The details about the parametrization and validation of our LGH model can be found in the Supporting Information. In Figure 3b we show the average binding energies per S atom obtained with the LGH model, ε^{LGH}, for structures with the same periodicities considered in Figure 3a and also for (6×6) structures. The close agreement with the available DFT results provides strong support to our LGH model. The agreement between DFT and LGH average binding energies is good not only for the structures considered during the optimization of the LGH model but also for various extra configurations we have used for test purposes. In particular, in Figure 3 we have included the average binding energy for the *rosette* motif with a (6×6) periodicity (open diamonds) for which the difference between the DFT and LGH values is ~0.01 eV (i.e., similar to the estimated error of the DFT values). The lowest energy LGH (6×6) curve being above the

dx.doi.org/10.1021/jp408340d | J. Phys. Chem. C 2014, 118, 290−297

one for (5 × 5) provides further support to the latter periodicity as the most stable one for the S/Au(111) system in a wide range of (low) S coverages.

Now, it is important to investigate to what extent the present theoretical lowest energy structures produce LEED patterns similar to the split-$\sqrt{3}$ pattern observed in the experiments.[6,14,15] With this aim, we have simulated the LEED patterns that would produce all the lowest energy structures characterized by a (5 × 5) periodicity.[39] In Figure 5 we show an experimental split-$\sqrt{3}$ LEED pattern (Figure.5a) and the simulated LEED patterns of the lowest energy structures with θ = 7/25, 6/25, and 5/25 (Figure 5b–d, respectively).[40]

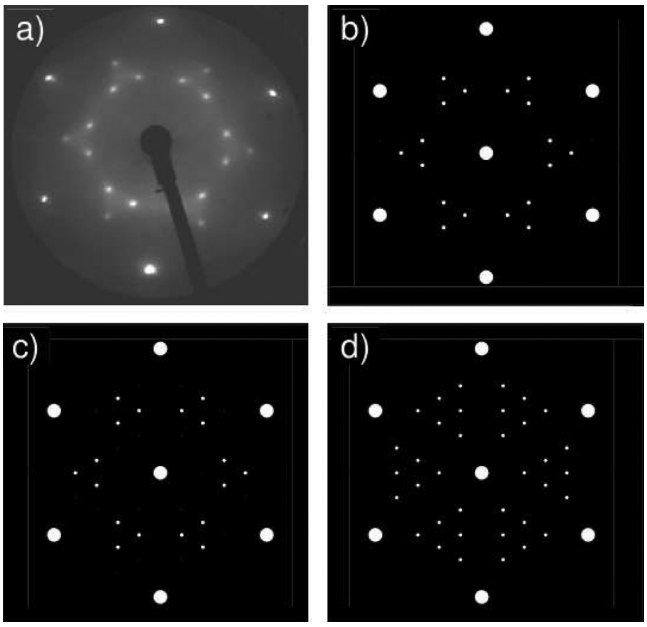

Figure 5. Comparison of LEED patterns. (a) Experimental LEED pattern (taken from ref 6). (b–d) simulated LEED patterns corresponding to the lowest energy (5 × 5) configurations with 7, 6, and 5 S atoms per unit cell, respectively. The relative sizes of the spots in the simulated patterns reflect the relative intensities.

As already pointed out in ref 6, the 7 S rosette motif with (5 × 5) periodicity gives rise to a split-$\sqrt{3}$ LEED pattern very similar to the experimental one. It can be seen in Figure 5 that, while the LEED pattern of the lowest energy structure with θ = 6/25 is still similar to the experimental pattern, the pattern of the lowest energy structure with θ = 5/25 presents some clear differences. Interestingly, this same situation is encountered with the lowest energy structures with θ = 4/25 and 3/25 (not shown in the figure). Accordingly, the present theoretical results predict that the split-$\sqrt{3}$ LEED pattern is expected to prevail in the coverage range $(6/25 + 5/25)/2 = 0.22 \leq \theta \leq 0.31$, while at lower coverages other patterns might be observable. However, since for the coverages θ = 5/25, 4/25, and 3/25 there are several configurations with ε^{DFT} values only ∼10 meV higher (less stable) than the absolute lowest energy configuration (see Table 2 in Supporting Information), the most probable event may be the observation of a superposition of patterns corresponding to different structures.

The existence of various configurations with energies close to that of the ground state mentioned above is not particular for this system. For relatively large unit cells and number of adsorbates, in general there are various possible structures differing from each other by the position of a few adsorbates which necessarily entails very similar average binding energies per adsorbate. Therefore, the *success* of the present DFT calculations to account for the experimental larger stability of (5 × 5) structures compared with $(\sqrt{3} \times \sqrt{3})R30°$ (under changes of S coverage) is remarkable.

In Table 1 we report the corresponding theoretical average heights of the S atoms above the closest extended ideal bulk

Table 1. S–Au Interlayer Spacing Relative to the Nearest Extended Bulk (111) Substrate Plane (h_S) for the GS Structures

θ	h_S (Å)
2/25	1.53
3/25	1.55
4/25	1.57
5/25	1.59
6/25	1.61
7/25	1.62
1/3	1.63

Au(111) plane, h_S, as obtained in NIXSW experiments. It is observed that h_S increases when θ increases, but all the values are very close to each other and to the experimental value: ∼(1.6 ± 0.1) Å.[6,41] In addition, the experimentally estimated average distance between S atoms and their closest Au atoms, ∼2.3 Å, is in good agreement with the theoretical value of 2.4 Å we have obtained irrespective of θ. Finally, good agreement between the theoretical and the experimental results is obtained for the average distance between the two outermost Au layers: ∼2.44 Å vs (2.36 ± 0.10) Å.[15]

The LGH model which we have mainly used to explore the stability of structures with periodicity (6 × 6), can also provide useful information on the S–S lateral interactions. With this aim, for simplicity we will analyze only the two-body S–S interactions of the LGH model. This is well justified because the relative stability of the *families* of structures characterized by different periodicities is not altered if the three-body terms of the LGH model are set equal to zero (see the Supporting Information for details).

In Figure 6 we show the two-body interaction energies, V_p, for all the S–S neighbor orders, p = 1,...14, considered in the LGH model as a function of the S–S distance d_p. The main features of this effective two-body interaction (from long to short S–S distances) are:

(i) small attraction (V_p ∼−5 meV) for p = 11 and 12 (i.e., for $d_p = 5\Delta \approx 15$ Å),
(ii) long-range repulsive character which decreases beyond the 5th-neighbor order ($V_5 \approx 60$ meV),
(iii) relatively small repulsion for 2NN S–S interactions (V_2 = 10 meV), and
(iv) strong repulsion between 1NN S atoms ($V_1 \approx 200$ meV).

The V_p interactions for $p \geq 9$ might be thought to be unimportant due to their very small values. To clarify this, we have computed the binding energy per S atom using the LGH model but setting equal to zero all the two-body terms V_p with $p \geq 9$, i.e. removing the feature (i) of pair S–S interaction. Such calculations predict a relative stability of the different *families* of structures quite different from the DFT one (see Supporting Information, Figure 3). In particular, the structures with periodicity $(3\sqrt{3} \times 3\sqrt{3})R30°$ become more stable than the

dx.doi.org/10.1021/jp408340d | J. Phys. Chem. C 2014, 118, 290–297

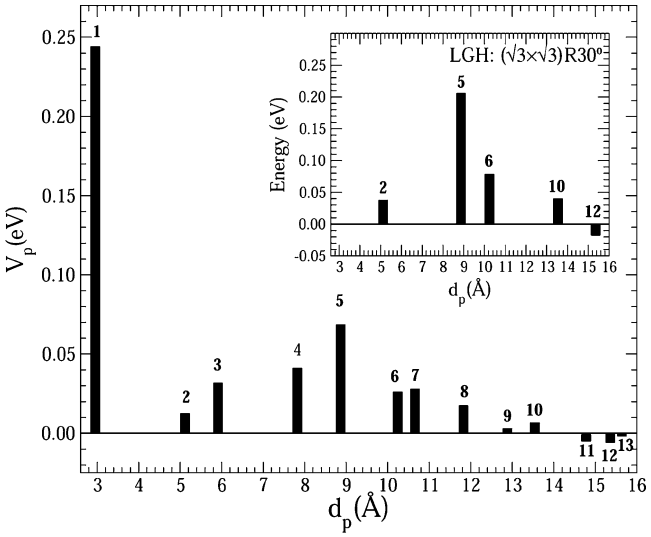

Figure 6. Two-body interaction energies, V_p, for all the S−S neighbor orders, p = 1,...14, considered in the LGH model as a function of the S−S distance d_p (numbers in bold denote the p values). Inset: Contribution to ε^{LGH} of the different pth-order pair interactions in the case of the $(\sqrt{3} \times \sqrt{3})R30°$ structure.

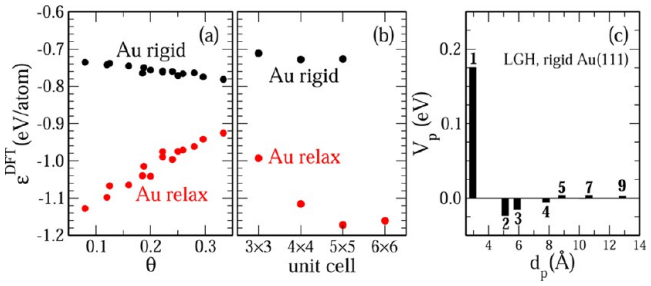

Figure 7. (a) Adsorption energies for the most stable configurations at each coverage for (•) fully relaxed and (•, red) rigid surface models. (b) Adsorption energy for a single S atom in the supercells (3 × 3), (4 × 4), (5 × 5), and (6 × 6) with (•) and without (•, red) allowing surface atoms relaxation upon adsorption. (c) Two-body S−S interactions of the LGH model developed from calculations where the elastic response of the Au(111) is switched off.

(5 × 5) ones, in contrast with DFT and full LGH results. This indicates that, in spite of their small size, the effective S−S pair attraction terms for 13 Å $\lesssim d_p \lesssim$ 17 Å play an important role for the energetics obtained with the LGH model and in particular, on the high stability of (5 × 5) structures.

To investigate the origin of the relatively low stability of the $(\sqrt{3} \times \sqrt{3})R30°$ structure discussed above, we have evaluated the contribution to ε^{LGH}, of the different pth-order pair interactions. The results are reported in the inset of Figure 6 which shows that the main positive contribution to ε^{LGH} comes from the 5th-order pair interactions (for $d_p = 3\Delta \approx 9$ Å). In particular, this contribution is larger than the one due to 2NN S atoms (p = 2) by a factor of ∼4−5. This suggests that the relatively low stability of the $(\sqrt{3} \times \sqrt{3})R30°$ structure is mainly due to the particularly large repulsion between S atoms placed at $3\Delta \approx 9$ Å from each other.

Now, we will address the origin of the repulsive V_p terms for 9 Å $\lesssim d_p \lesssim$ 13 Å. On the one hand, it might be a consequence of the direct electrostatic repulsion between adsorbates since, in line with previous theoretical results,[1] our Bader charge analysis shows that ∼0.26 e are transferred from the Au(111) surface to each S atom (irrespective of the S coverage $1/9 \leq \theta \leq 1/3$). On the other hand, such repulsive V_p terms might be the consequence of an indirect surface-mediated interaction due to the local strain (and the consequent Au atom rearrangement) produced by S atoms. To clarify this issue, we have carried out calculations for several structures, keeping the surface atoms frozen in their equilibrium positions for the clean surface and, thus, only optimizing the geometry of the S atoms.[42] The resulting ε values obtained within this rigid surface model are compared with the full geometry optimization results for the *same* configurations in Figure 7. In panel a, we have plotted the DFT average binding energies per S atom as a function of coverage. The effect of preventing surface relaxation upon adsorption is dramatic. Whereas for the rigid Au(111) surface model, ε^{DFT} slightly decreases when θ increases, it strongly increases when surface relaxation is allowed. In Figure 7 b we compare the binding energy for a single S atom in the supercells (3 × 3), (4 × 4), (5 × 5), and (6 × 6) with and without allowing surface atoms relaxation upon adsorption. Whereas for the rigid surface the binding energy does not depend on the cell size, when surface relaxation is allowed, the binding energy for the (3 × 3) cell is ∼0.15 eV larger (adsorption is less stable) than for the cells (5 × 5) and (6 × 6). In Figure 7c, we show the two-body interactions of a new LGH with on-site, and pair interactions only, parametrized using the binding energies obtained within the rigid surface model. The results of panels b and c of Figure 7 show that in the case of a rigid surface model there is an almost negligible interaction between S atoms separated beyond ∼3Δ. This contrasts with the behavior of the V_p parameters of the LGH model shown in Figure 6. Thus, all these results show a prominent and surprisingly large effect of substrate relaxation pointing to surface-mediated elastic interactions as the main driving force for the long-range S−S repulsion observed in Figure 6 for 9 Å $\lesssim d_p \lesssim$ 13 Å ($5 \leq p \leq 10$).

When the contribution of the elastic response of the Au(111) is switched off (rigid surface model), the pair interactions V_p of the LGH model for $2 \leq p \leq 4$ are negative (attractive interaction between adsorbates). Interestingly, for $p \leq 5$, the V_p values obtained for the rigid surface model seem to be simply shifted down by ∼50 meV with respect to the ones shown in Figure 6, but roughly preserving the relative values corresponding to different p-orders. This suggests that for 5 Å $\lesssim d_p \lesssim$ 9 Å, the lateral interactions (Figure 6) are due to the additive contribution of repulsive surface-mediated elastic interactions and an attractive S−S interaction (observed with and without surface relaxation). This attraction is certainly not due to van der Waals interactions which are not included in our DFT-GGA calculations.[43] On the other hand, the Bader charges obtained for S coverages θ = 1/9, 1/4, and 1/3 (i.e., for 1NN S−S distances ∼9 Å, 6 Å, and 5 Å, respectively) are very similar to each other. Therefore, the S−S attraction observed for $d_{S-S} \approx$ 5−6 Å (Figure 7c) cannot be unambiguously linked to a charge redistribution in the rigid Au surface induced by the S atoms and might be due to other relatively subtle electronic effects. Finally, the strongly repulsive feature (iv) of the S−S interaction for 1NN S adsorbates is most likely due to a dominant direct electrostatic interaction between S atoms which takes ∼0.26 e from the surface.

dx.doi.org/10.1021/jp408340d | J. Phys. Chem. C 2014, 118, 290−297

CONCLUSIONS

In this work, we have investigated the adsorption of sulfur on Au(111) at low and intermediate coverages ($\theta \leq 1/3$) by means of a systematic analysis based on DFT calculations. Our calculations predict a ground state curve characterized by two periodicities: (5 × 5) and $(\sqrt{3} \times \sqrt{3})R30°$. In line with experiments, the (5 × 5) periodicity seems to dominate in a much larger coverage range than the $(\sqrt{3} \times \sqrt{3})R30°$ one, which should be only observable in a narrow coverage window close to 1/3. Besides, we have also found that the experimentally observed split-$\sqrt{3}$ LEED pattern is expected to prevail in the coverage range $0.31 \leq \theta \leq 0.33$. Finally, our results unambiguously highlight the prominent and surprising role of S-induced substrate relaxation on the complex nature of the S−Au interface. Through a first-principles parametrized lattice-gas Hamiltonian approach, we determine lateral interactions between S atoms whose main features are: (i) slight attraction for S−S distances $d_{S-S} \approx 15$ Å favoring 5 × 5 arrangements, (ii) shorter but still long-ranged S−S repulsion due to the elastic response of the Au(111) surface, which is maximum for $d_{S-S} \approx 9$ Å, and being the major source of instability of the $(\sqrt{3} \times \sqrt{3})R30°$ structure, (iii) very small repulsion at $d_{S-S} \approx 5$ Å which helps to understand the high stability of the *rosette-like* motif, and (iv) large short-range (presumably electrostatic) repulsion (i.e., $d_{S-S} \approx 3$ Å) which prevents structures with first nearest neighbor S atoms.

Further calculations including the effect of the temperature are the subject of our present research.

ASSOCIATED CONTENT

Supporting Information

Full description of DFT and LGH calculations. This material is available free of charge via the Internet at http://pubs.acs.org.

AUTHOR INFORMATION

Corresponding Author

*To whom correspondence should be addressed E-mail: abufager@ifir-conicet.gov.ar,Phone:+543414495467.

Notes

The authors declare no competing financial interest.

ACKNOWLEDGMENTS

This work has been supported by ANPCyT-Argentine (Projects No. PICT-2010-1962 and PICT-2008-1260), CONICET (Project No. PIP 0667) and UNR (Project No. PID ING235).

REFERENCES

(1) Rodriguez, J. A.; Dvorak, J.; Jirsak, T.; Liu, G.; Hrbek, J.; Aray, Y.; González, C. Coverage Effects and the Nature of the Metal−Sulfur Bond in S/Au(111): High-Resolution Photoemission and Density-Functional Studies. *J. Am. Chem. Soc.* **2003**, *125*, 276−285.

(2) Carro, P.; Corthey, G.; Rubert, A. A.; Benitez, G. A.; Fonticelli, M. H.; Salvarezza, R. C. The Complex Thiol-Palladium Interface: A Theoretical and Experimental Study. *Langmuir* **2010**, *26*, 14655−14662.

(3) Thomas, J. P.; Zhao, L.; Ding, K.; Heinig, N. F.; Leung, K. T. Near-Surface Oxidized Sulfur Modifications and Self-Assembly of Thiol-Modified Aptamer on Au Thin Film Substrates Influenced by Piranha Treatment. *ACS Appl. Mater. Interfaces* **2012**, *4*, 5945−5948.

(4) Vericat, C.; Andreasen, G.; Vela, M.; Salvarezza, R. Dynamics of Potential-Dependent Transformations in Sulfur Adlayers on Au(111) Electrodes. *J. Phys.Chem. B.* **2000**, *104*, 302−307.

(5) Gao, X.; Zhang, Y.; Weaver, M. J. Observing Surface Chemical Transformations by Atomic-Resolution Scanning Tunneling Microscopy: Sulfide Electrooxidation on Gold(111). *J. Phys. Chem.* **1992**, *96*, 4156−4159.

(6) Yu, M.; Ascolani, H.; Zampieri, G.; Woodruff, D. P.; Satterley, C. J.; Jones, R. G.; Dhanak, V. R. The Structure of Atomic Sulfur Phases on Au(111). *J. Phys. Chem. C* **2007**, *111*, 10904−10914.

(7) Heinz, R.; Rabe, J. P. Scanning Tunneling Microscopy Investigation of Sulfide and Alkanethiolate Adlayers on Ag(111). *Langmuir* **1995**, *11*, 506−511.

(8) Quek, S. Y.; Biener, M. M.; Biener, J.; Bhattacharjee, J. Rich Coordination Chemistry of Au Adatoms in Gold Sulfide Monolayer on Au(111). *J. Phys. Chem. B* **2006**, *110*, 15663−15665.

(9) Vericat, C.; Vela, M.; Benitez, G. A.; Gago, J. A. M.; Torrelles, X.; Salvarezza, R. C. Surface Characterization of Sulfur and Alkanethiol Self-Assembled Monolayers on Au(111). *J. Phys.: Condens. Matter* **2006**, *18*, R867−R900.

(10) Biener, M. M.; Biener, J.; Friend, C. M. Revisiting the S−Au(111) Interaction: Static or Dynamic? *Langmuir* **2005**, *21*, 1668−1671.

(11) Lustemberg, P. G.; Vericat, C.; Benitez, G. A.; Vela, M. E.; Tognalli, N.; Fainstein, A.; Martiarena, M. L.; Salvarezza, R. C. Spontaneously Formed Sulfur Adlayers on Gold in Electrolyte Solutions: Adsorbed Sulfur or Gold Sulfide. *J. Phys. Chem. C* **2008**, *112*, 11394−11402.

(12) Quek, S. Y.; Biener, M. M.; Biener, J.; Bhattacharjee, J.; Friend, C. M.; Waghmare, U. V.; Waghmare, U. V.; Kaxiras, E. Structure of Incommensurate Gold Sulfide Monolayer on Au(111). *J. Chem. Phys.* **2007**, *127*, 104704-1−104704-7.

(13) Koczkur, K. M.; Hamed, E. M.; Houmam, A. Sulfur Multilayer Formation on Au(111): New Insights from the Study of Hexamethyldisilathiane. *Langmuir* **2011**, *27*, 12270−12274.

(14) Biener, M.; Biener, J.; Friend, C. M. Sulfur-Induced Mobilization of Au Surface Atoms on Au(111) Studied by Real-Time STM. *Surf. Sci.* **2007**, *601*, 1659−1667.

(15) McGuirk, G.; Shin, H.; Caragiu, M.; Ash, S.; Bandyopadhyay, P.; Prince, R.; Diehl, R. Au(111) Surface Structures Induced by Adsorption: LEED I(E) Analysis of (1 × 1) and (5 × 5) Au(111)S phases. *Surf. Sci.* **2013**, *610*, 42−47.

(16) Sanchez, J. M.; Ducastelle, F.; Gratias, D. Generalized Cluster Expansion Description of Multicomponent Systems. *Physica A* **1984**, *128*, 334−350.

(17) Zunger, A. *Statics and Dynamics of Alloy Phase Transformations*; Plenum Press: New York, 1994; pp 361−419.

(18) Stampfl, C.; Kreuzer, H. J.; Payne, S. H.; Pfnür, H.; Scheffler, M. First-Principles Theory of Surface Thermodynamics and Kinetics. *Phys. Rev. Lett.* **1999**, *83*, 2993−2996.

(19) Drautz, R.; Singer, R.; Fähnle, M. Cluster Expansion Technique: An Efficient Tool to Search for Ground-State Configurations of Adatoms on Plane Surfaces. *Phys. Rev. B* **2003**, *67*, 035418-1−035418-4.

(20) Fähnle, M.; Drautz, R.; Lechermann, F.; Singer, R.; Diaz-Ortiz, A.; Dosch, H. Thermodynamic Properties from Ab-Initio Calculations: New Theoretical Developments, and Applications to Various Materials Systems. *Phys. Status Solidi B* **2005**, *242*, 1159−1173.

(21) Zhang, Y.; Blum, V.; Reuter, K. Accuracy of First-Principles Lateral Interactions: Oxygen at Pd(100). *Phys. Rev. B* **2007**, *75*, 235406−1−235406−14.

(22) Stöhr, M.; Podloucky, R.; Müller, S. Ab Initio Phase Diagram of Oxygen Adsorption on W(110). *J. Phys.: Condens. Matter* **2009**, *21*, 134017.

(23) In this context, ε_i refers to the average binding energy per adsorbate for a single domain i that covers the whole surface.

(24) Jansen, A. Island Formation without Attractive Interactions. *Phys. Rev. B* **2008**, *77*, 073408−1−073408−4.

(25) Perdew, J. P.; Wang, Y. Accurate and Simple Analytic Representation of the Electron-Gas Correlation Energy. *Phys. Rev. B* **1992**, *45*, 13244−13249.

(26) Kresse, G.; Hafner, J. Ab Initio Molecular Dynamics for Liquid Metals. *Phys. Rev. B* **1993**, *47*, 558−561.
(27) Kresse, G.; Hafner, J. Ab Initio Molecular Dynamics for Open-Shell Transition Metals. *Phys. Rev. B* **1993**, *48*, 13115−13118.
(28) Kresse, G.; Furthmüller, J. Efficiency of Ab-Initio Total Energy Calculations for Metals and Semiconductors Using a Plane-Wave Basis Set. *Comput. Mater. Sci.* **1996**, *6*, 15−50.
(29) Kresse, G.; Furthmüller, J. Efficient Iterative Schemes for Ab Initio Total-Energy Calculations Using a Plane-Wave Basis Set. *Phys. Rev. B* **1996**, *54*, 11169−11186.
(30) Kresse, G.; Joubert, D. From Ultrasoft Pseudopotentials to the Projector Augmented-Wave Method. *Phys. Rev. B* **1999**, *59*, 1758−1775.
(31) Hafner, J. Ab-Initio Simulations of Materials Using VASP: Density-Functional Theory and Beyond. *J. Comput. Chem.* **2008**, *29*, 2044−2078.
(32) Vanderbilt, D. Soft Self-Consistent Pseudopotentials in a Generalized Eigenvalue Formalism. *Phys. Rev. B* **1990**, *41*, 7892−7895.
(33) Monkhorst, H.; Pack, D. Special Points for Brillouin-Zone Integrations. *Phys. Rev. B* **1976**, *13*, 5188−5192.
(34) Methfessel, M.; Paxton, A. T. High-Precision Sampling for Brillouin-Zone Integration in Metals. *Phys. Rev. B* **1989**, *40*, 3616−3621.
(35) Kittel, C. *Introduction to Solid State Physics*; New York, John Wiley & Sons: New York, 1971.
(36) Alfonso, D. R. First-Principles Studies of H_2S Adsorption and Dissociation on Metal Surfaces. *Surf. Sci.* **2008**, *602*, 2758−2768.
(37) We focus our analysis on $\theta \gtrsim 0.1$ because for lower coverages, S adsorption is influenced by the herringbone reconstruction of Au(111),[14] or takes places preferentially on surface defects (e.g., steps).[10]
(38) Note that the ground state structure corresponding to $\theta = 5/25$ is also characterized by a shorter-range periodicity: $(\sqrt{3} \times \sqrt{7})$.
(39) For each coverage, we have considered all the structures characterized by average binding energies up to 0.01 eV higher than the absolute lowest energy structures.
(40) The intensities were calculated with a simple kinematical model for a single layer of S atoms, with the atoms treated as isotropic scatterers. All the simulated patterns have been averaged over the three equivalent domains rotated 120°.
(41) h_S compares well also with the S−Au average interlayer spacing estimated from LEED analysis.[15]
(42) This procedure was carried out for all the most stable structures found for each coverage.
(43) This shortcoming of DFT-GGA does not affect the present discussion since, according to the DFT-D2 model proposed by Grimme,[44] the S−S dispersion correction for $d_{S-S} = 5$ Å is 1 order of magnitude smaller than the corresponding V_p value observed in Figure 7c.
(44) Grimme, S. Semiempirical GGA-type Density Functional Constructed with a Long-Range Dispersion Correction. *J. Comput. Chem.* **2006**, *27*, 1787−1799.